Wide Bandwidth Observations of Pulsars C, D, and J in 47 Tucanae

Lei Zhang[1,2,3] , George Hobbs[1,3], Richard N. Manchester[3] , Di Li[1,2,4] , Pei Wang[1], Shi Dai[1,3] , Jingbo Wang[5] ,
Jane F. Kaczmarek[3], Andrew D. Cameron[1,3], Lawrence Toomey[3], Weiwei Zhu[1], Qijun Zhi[6,7], Chenchen Miao[1,2], Mao Yuan[1,2],
Songbo Zhang[2,3,8,9] , and Zhenzhao Tao[1,6,7]

[1] National Astronomical Observatories, Chinese Academy of Sciences, A20 Datun Road, Chaoyang District, Beijing 100101, People's Republic of China;
leizhang996@nao.ac.cn, dili@nao.cas.cn
[2] University of Chinese Academy of Sciences, Beijing 100049, People's Republic of China
[3] CSIRO Astronomy and Space Science, P.O. Box 76, Epping, NSW 1710, Australia
[4] FAST Collaboration, CAS Key Laboratory of FAST, NAOC, Chinese Academy of Sciences, Beijing 100101, People's Republic of China
[5] Xinjiang Astronomical Observatory, 150, Science-1 Street, Urumqi, 830011 Xinjiang, People's Republic of China
[6] Guizhou Provincial Key Laboratory of Radio Astronomy and Data Processing, Guizhou Normal University, Guiyang, 550001, People's Republic of China
[7] School of Physics and Electronic Science, Guizhou Normal University, Guiyang, 550001, People's Republic of China
[8] Purple Mountain Observatory, Chinese Academy of Sciences, Nanjing 210008, People's Republic of China
[9] International Centre for Radio Astronomy Research, University of Western Australia, Crawley, WA 6009, Australia

Abstract

We report the first wide-band observations of pulsars C, D, and J in the globular cluster 47 Tucanae (NGC 104) using the Ultra-Wideband Low (UWL) receiver system recently installed on the Parkes 64 m radio telescope. The wide frequency range of the UWL receiver (704–4032 MHz), along with the well-calibrated system, allowed us to obtain flux density measurements and polarization pulse profiles. The mean pulse profiles have significant linear and circular polarization, allowing for determination of the Faraday rotation measure for each pulsar. Precise measurements of the dispersion measures show a significant deviation in the value for pulsar D compared to earlier results. Searches for new pulsars in the cluster are ongoing and we have determined optimal bands for such searches using the Parkes UWL receiver system.

1. Introduction

With 25 known radio pulsars, 47 Tucanae (47 Tuc or NGC 104) is the second most populous globular cluster in terms of number of known pulsars. All the pulsars were discovered using the Parkes 64 m radio telescope at a wavelength of 20, 50, or 70 cm (Manchester et al. 1990, 1991; Robinson et al. 1995; Camilo et al. 2000; Lorimer et al. 2003; Knight 2007; Pan et al. 2016). All 25 are millisecond pulsars with spin periods smaller than 8 ms and 15 are in binary systems. McConnell & Ables (2000) made Australia Telescope Compact Array (ATCA) radio images of the cluster at 1.4 and 1.7 GHz; they detected 11 point sources within 5′ of the cluster center and the positions of three of them can be identified with 47 Tuc C, D, and J (Freire et al. 2001).[10] Measured flux densities are extremely variable, mainly because of scintillation (Rickett 1977), but also because some of the binary pulsars show eclipses of the radio emission by circumstellar gas (e.g., 47 Tuc J; see Robinson et al. 1995 for more details). Camilo et al. (2000) reported that most pulsars in 47 Tuc are visible only when the pulsar signals are amplified by scintillation. They estimated mean flux densities of the pulsars in 47 Tuc at 20 cm by assuming that scintillation effects are similar for all pulsars. To date, 14 pulsars in 47 Tuc have known flux densities measured at 436 MHz, 640 MHz, and/or 1400 MHz from the Parkes telescope (Robinson et al. 1995; Camilo et al. 2000). 47 Tuc C, D, and J have flux densities measured at 1400 and 1700 MHz from ATCA (McConnell & Ables 2000). The most recent timing models for 22 of the known pulsars in the cluster were presented by Ridolfi et al. (2016) and Freire et al. (2017)

using data taken in the 20 cm (1400 MHz) observing band with the multibeam receiver on the Parkes radio telescope (Staveley-Smith et al. 1996). There are no previous wide-band or well-calibrated polarization observations of pulsars in 47 Tuc.

Here we present observations of 47 Tuc using the Ultra-Wideband Low (UWL) receiver system recently installed at the Parkes radio telescope (Hobbs et al. 2019). This receiver covers the band 704–4032 MHz with excellent sensitivity and polarization properties. We report wide-band flux density measurements and spectral properties (Section 3.1), updated measurements of dispersion measures (DMs; Section 3.2), and polarization pulse profiles along with Faraday rotation measures (RMs; Section 3.3) for pulsars C, D, and J in 47 Tuc.

2. Observations and Data Reduction

Pulsar observations of 47 Tuc have often used a "search" mode, where multiple frequency channels are rapidly sampled, typically with sample intervals of order 100 μs. This enables both searches for previously unknown pulsars in the cluster and the study of multiple pulsars with a given observation. However, such observations generally have restricted pulse phase, frequency, and polarization information and often use few-bit digitization, reducing their sensitivity and dynamic range. In contrast, we can observe a specific pulsar in the cluster using the fold-mode capability. This leads to a better-defined pulse profile that can be accurately calibrated in both polarization and flux density. We have therefore obtained multiple fold-mode observations of three of the brightest 47 Tuc pulsars (C, D, and J) that cover the entire band of the UWL receiver.

---

[10] Also known as PSRs J0024−7204C, J0024−7204D, and J0024−7204J.

Table 1
Observations of 47 Tuc C, D, and J

Pulsar	Date (MJD)	Duration (s)	N_{bin}	File Name
47 Tuc C	58583.13	3348	1024	uwl_190410_031517_b4.rf
	58586.93	7278	1024	uwl_190413_222147_b4.rf
	58602.77	10430	512	uwl_190429_183836_b4.rf
	58671.82	4114	512	uwl_190707_194346_b4_0.rf
	58671.86	4106	512	uwl_190707_194346_b4_1.rf
	58677.67	5213	512	uwl_190713_161547_b4_0.rf
	58677.73	5220	512	uwl_190713_161547_b4_1.rf
	58677.79	5232	512	uwl_190713_161547_b4_2.rf
47 Tuc D	58583.22	2478	1024	uwl_190410_052207_b4.rf
	58587.12	3734	512	uwl_190414_025617_b4.rf
	58602.89	5529	512	uwl_190429_213437_b4.rf
	58669.66	4040	512	uwl_190705_160226_b4.rf
	58669.78	4510	512	uwl_190705_184456_b4.rf
	58674.79	5384	512	uwl_190710_190536_b4_0.rf
	58674.85	5402	512	uwl_190710_190536_b4_1.rf
	58677.86	4014	512	uwl_190713_203906_b4_0.rf
	58677.90	4020	512	uwl_190713_203906_b4_1.rf
	58677.95	4016	512	uwl_190713_203906_b4_2.rf
47 Tuc J	58663.76	4463	512	uwl_190629_181617_b4_0.rf
	58663.81	4480	512	uwl_190629_181617_b4_1.rf
	58663.86	4506	512	uwl_190629_181617_b4_2.rf
	58672.72	5613	512	uwl_190708_172027_b4_0.rf
	58672.78	5620	512	uwl_190708_172027_b4_1.rf
	58672.85	5602	512	uwl_190708_172027_b4_2.rf
	58678.67	5134	512	uwl_190714_160846_b4_0.rf
	58678.73	5136	512	uwl_190714_160846_b4_1.rf

A summary of the observations is given in Table 1, which lists the pulsar name, the observing date, the observation length, the number of pulse phase bins, and the corresponding file name. The data for all observations were coherently de-dispersed and channelized with 1 MHz channels, integrated for 20 s, and then written to disk. Each observation was preceded by a short (1 minute) observation with a pulsed calibration signal injected into the low-noise amplifiers (see Hobbs et al. 2019 for more details). Some early observations had 1024 bins per period; these were reduced to 512 bins as a first stage of the signal processing for consistency with the rest of the data sets. We removed 5 MHz at each edge of each of the 26 sub-bands to avoid the effects of aliasing (see Hobbs et al. 2019 for more details) and then manually excised data affected by radio frequency interference (RFI) in frequency and time for each channel and subintegration.

To transform the measured intensities to absolute flux densities, we used observations of the radio galaxy 3C 218 (Hydra A; see Xie et al. 2019 for more details). We measured the flux density for each pulsar by first forming noise-free standard templates using the PSRCHIVE program PAAS and then using PSRFLUX to cross-correlate the observed profile with the standard template to obtain a scaling factor and then the average flux density. The uncertainty of the flux density is estimated as the rms noise of the profile baseline.

We calibrated the polarization response of the UWL feed using multiple observations of the bright millisecond pulsar PSR J0437−4715 that covered a wide range of parallactic angles (van Straten 2004). To probe the polarimetric properties for each pulsar, we created a weighted sum of the 128 MHz sub-band pulse profiles. Determining the signal-to-noise ratio

(S/N) of a low-S/N profile is prone to biases. Therefore, sub-band pulse profiles in which the S/N was less than 10 were not included in the summation. The pulsars are weak in the higher bands and so our final pulse profiles covered a band between 704 and 2240 MHz. We determined the RM of the pulsars over this 1536 MHz bandwidth, using the RMFIT package. The measured RMs were then used to refer all PAs to the overall band center, 1472 MHz, before summing to form the polarization profiles.

In order to determine the DM for each pulsar, we generated times of arrival (ToAs) from all combined observations. These ToAs were obtained by splitting the profiles into 12 unequal sub-bands defined by four groups: seven sub-bands from 704 to 1728 MHz, two sub-bands from 1728 to 2240 MHz, two sub-bands from 2240 to 3264 MHz, and one sub-band from 3264 to 4032 MHz. We used the same noise-free standard template that was used when measuring the flux densities. The TEMPO2 (Hobbs et al. 2006) software package was subsequently used to fit for the DM.

The observations from the Parkes radio telescope have been obtained under project codes P1006 and PX500. Conditional on data embargoes, these data are available on CSIRO's data archive[11] (Hobbs et al. 2011)—the raw P1006 and PX500 data have an 18-month embargo period. We have also produced a publicly downloadable data collection containing our processed data files[12] (Zhang et al. 2019). This data collection contains (1) the raw files of multiple fold-mode observations, (2) the calibration files, (3) the calibrated and RFI-removed profiles, and (4) the flux and polarization calibrated files for these three pulsars.

3. Results and Discussion

3.1. Flux Density Measurements and Spectral Properties

We present the flux density measurements for 47 Tuc C, D, and J determined from 26 sub-bands (each with a 128 MHz bandwidth) over the whole frequency band in Table 2 and shown in Figure 1. Each panel contains three solid lines. For 47 Tuc C, these correspond to flux densities from all combined observations (labeled "all"), the observations obtained in April (labeled "obs1"), and the observations obtained in July (labeled "obs2"). For 47 Tuc D and J the three lines correspond to the average of all observations ("all"), a subset of "typical" observations ("obs1") and the observation in which the pulsar was brightest ("obs2"). For comparison, flux density estimates from previous work (Robinson et al. 1995; Camilo et al. 2000; McConnell & Ables 2000) are overlaid using blue cross and green star symbols.

These three pulsars have steep spectra. The spectra of 47 Tuc C can be best characterized as a log-parabolic spectrum (LPS). The form of the LPS is (Jankowski et al. 2018)

$$\log_{10} S_\nu = ax^2 + bx + c, \qquad (1)$$

where $x = \log_{10}(\nu/\nu_0)$, a is the curvature parameter, b is the spectral index for $a = 0$, and c is a constant. The fitted parameters, a, b, and c are $-2.6(3)$, $-4(2)$, and $-2(5)$ where uncertainties in parentheses refer to the last quoted digit from the 1σ level. The spectral fitting result is shown as the dotted–dashed line in the top panel of Figure 1. The spectra of 47 Tuc

---

Table 2
Flux Density Measurements, Dispersion Measures, Rotation Measures, and the Width of Pulse Profiles at 50% (W_{50}) and 10% (W_{10}) for 47 Tuc C, D, and J

	47 Tuc C	47 Tuc D	47 Tuc J
Flux Density (mJy)			
S_{768}	1.44(2)	1.06(3)	12.11(5)
S_{896}	1.02(3)	1.8(4)	6.90(4)
S_{1024}	1.31(1)	0.46(1)	4.93(1)
S_{1152}	0.88(1)	0.41(1)	1.32(1)
S_{1280}	0.88(1)	0.41(1)	0.88(1)
S_{1408}	0.52(1)	0.35(1)	0.44(1)
S_{1536}	0.53(1)	0.30(1)	0.31(1)
S_{1664}	0.50(1)	0.30(1)	0.27(1)
S_{1792}	0.26(1)	0.27(1)	0.29(1)
S_{1920}	0.23(1)	0.21(1)	0.31(1)
S_{2048}	0.23(1)	0.20(1)	0.20(1)
S_{2176}	0.16(1)	0.18(1)	0.17(1)
S_{2304}	0.16(1)	0.16(1)	0.17(1)
S_{2432}	0.10(1)	0.07(1)	0.14(1)
S_{2560}	0.12(1)	0.08(1)	0.10(1)
S_{2688}	0.11(1)	0.06(1)	0.12(1)
S_{2816}	0.08(1)	0.06(1)	0.12(1)
S_{2944}	0.06(1)	0.05(1)	0.10(1)
S_{3072}	0.07(1)	0.05(1)	0.10(1)
S_{3200}	0.03(1)	0.05(1)	0.09(1)
S_{3328}	0.05(1)	0.02(1)	0.08(1)
S_{3456}	0.01(1)	0.02(1)	0.07(1)
S_{3584}	0.04(1)	0.04(1)	0.06(1)
S_{3712}	0.03(1)	0.06(1)	0.07(1)
S_{3840}	0.04(1)	0.04(1)	0.05(1)
S_{3968}	0.06(1)	0.02(1)	0.06(1)
DM (cm^{-3} pc)			
Freire et al. (2017)	24.600(4)	24.732(3)	24.588(3)
This work	24.5955(8)	24.7432(9)	24.5932(1)
RM (rad m^{-2})^{a}	27(4)	28(4)	20(4)
W_{50} (deg)			
832 MHz	45.7	21.8	36.6
1152 MHz	41.5	20.4	35.9
1792 MHz	39.4	9.8	35.2
W_{10} (deg)			
832 MHz	75.9	49.2	63.3
1152 MHz	73.8	48.5	56.3
1792 MHz	71.7	46.4	54.8

Note. Uncertainties in parentheses refer to the last quoted digit.
[a] The RM uncertainties include the potential effect of ionospheric RM (Sobey et al. 2019).

Figure 1. Flux density as a function of frequency with 26 frequency sub-bands for 47 Tuc C (top panel), D (middle panel), and J (bottom panel). The blue cross symbols are the previously measured flux densities at 436, 640, and 1400 MHz for the pulsars from Parkes (Robinson et al. 1995; Camilo et al. 2000). The green star symbols are the previously measured flux densities at 1400 and 1700 MHz for the pulsars from ATCA (McConnell & Ables 2000). The legend indicates the color/line scheme used to represent the average of all observations or specific observations. The dashed and dotted–dashed lines represent the spectral fitting results. See the text in Section 3.1 for more details.

D can also be characterized as an LPS. The fitted parameters, a, b, and c are $-3.6(8)$, $-4(7)$, and $-1(2)$ (shown as the dotted–dashed line in the middle panel of Figure 1). We note that this LPS fit is strongly affected by the low-frequency flux density measurements at 436 and 640 MHz. If we only use the observations described in this Letter, then the spectrum can be characterized as a simple power law (Jankowski et al. 2018):

$$S_\nu = bx^\alpha, \qquad (2)$$

where $x = \nu/\nu_0$, α is the spectral index and b is a constant. The fitted parameters α and b are $-2.3(3)$ and $1(6)$. The spectral fitting result is shown as the dashed line in the figure.

For 47 Tuc J, we use a simple power law fitted to all sub-bands to measure a spectral index $\alpha = -4.7(3)$ with a constant
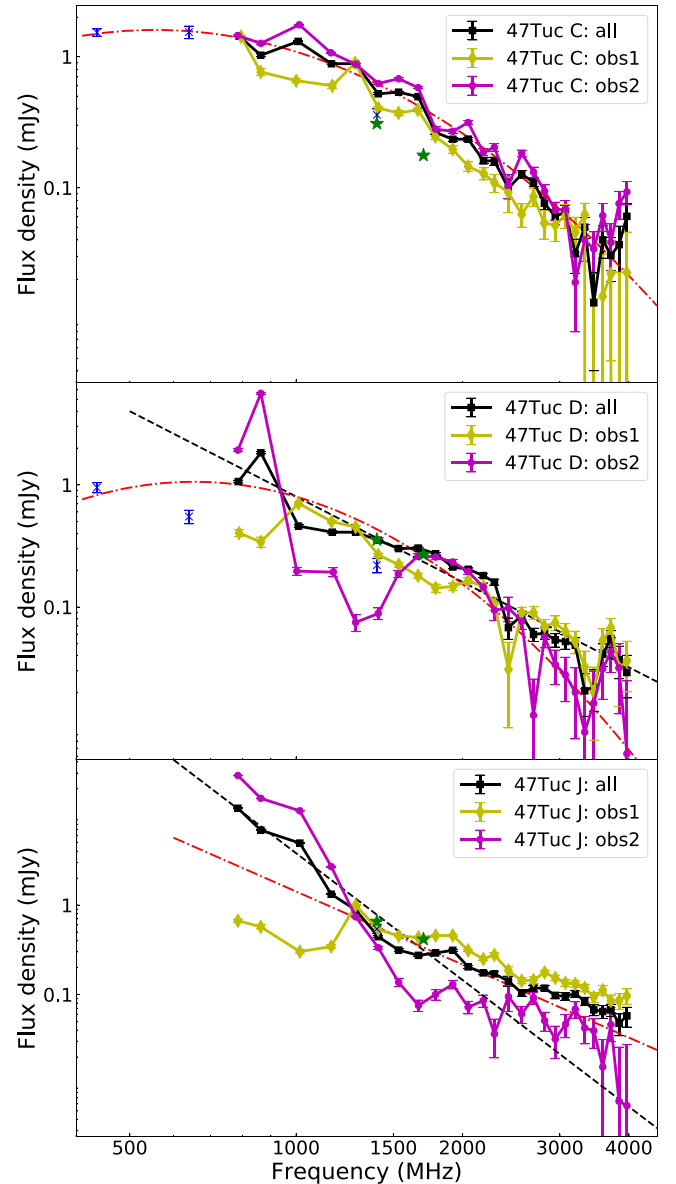
$b = 1(7)$ (shown as the dashed line in the bottom panel of Figure 1). However, the flux density fluctuations between observations result in large uncertainties and affect the fitting for the spectral index. Therefore, for comparison, we also fitted the bottom 22 frequency sub-bands without the first four bright sub-bands and obtained a spectral index of $\alpha = -2.7(3)$ with a constant $b = 1(5)$. The spectral fitting result is shown as a dotted–dashed line in the figure.

The results for 47 Tuc D and J are not surprising as Jankowski et al. (2018) reported that 79% of pulsar spectra can be characterized as a simple power law. However, pulsars exhibiting an LPS spectrum, such as 47 Tuc C, in this
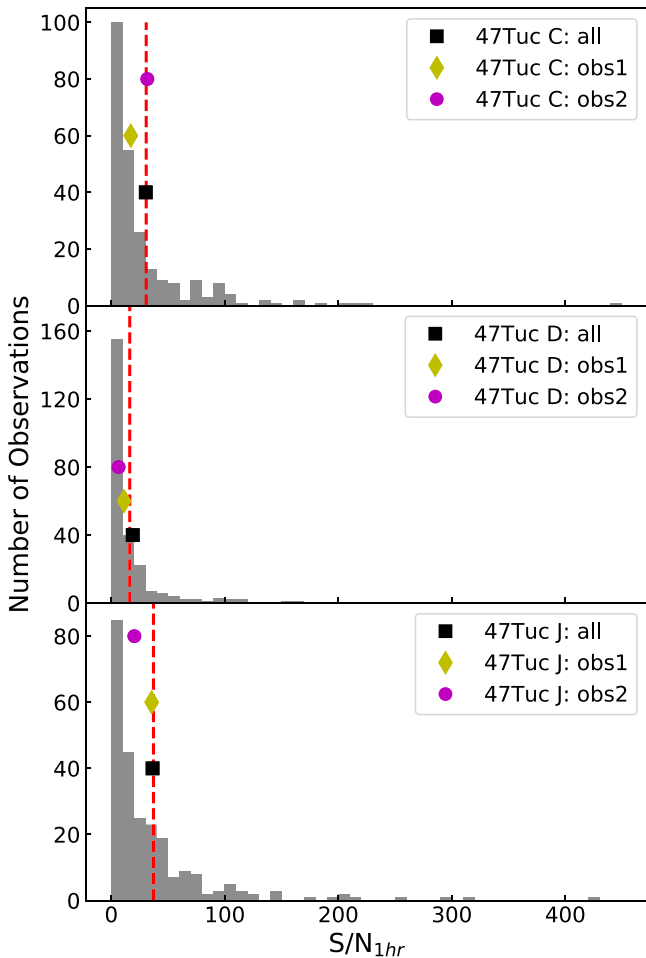
Figure 2. Histograms of the signal-to-noise ratio (S/N) per hour for 47 Tuc C (top panel), D (middle panel), and J (bottom panel). The distributions are the measured S/N at 1400 MHz with 256 MHz bandwidth for these three pulsars from previous Parkes surveys. Black square symbols show the S/N for all combined observations at 1400 MHz with 256 MHz bandwidth for the pulsars from this work. For 47 Tuc C, the yellow diamond and purple circle symbols show combined observations on April and July. For 47 Tuc D and J, the yellow diamond and purple circle symbols show combined observations from normal emission observations and bright observation. The red vertical dashed line marks the mean of S/N for the distribution of each pulsar.

frequency band are much less common (accounting for about 10% of the Jankowski et al. 2018 sample).

Scintillation is known to affect the measured flux densities of the pulsars in 47 Tuc significantly (Robinson et al. 1995; Camilo et al. 2000) and our results show, in some sub-bands, flux density variations of more than an order of magnitude relative to the median value. We can determine whether such variations are typical by comparing with the large number of observations of this cluster (spanning over 10 yr) present in the CSIRO data archive (Hobbs et al. 2011). We obtained 248 publicly available observations for 47 Tuc C, D, and J obtained in the 20 cm observing band with 256 MHz bandwidth. The duration of the observation for each data file varied from 1 to 7 hr. We scaled the measured S/N of the folded profile of each pulsar to the value that would have been obtained after a 1 hr observation. The distribution functions of S/N variations for these three pulsars are shown in Figure 2; standard deviations are 47.3, 24.5, and 53.5 for 47 Tuc C, D, and J, respectively. Our UWL results are consistent with these distributions.

Searches for new pulsars in 47 Tuc are ongoing and the Parkes UWL receiver system is ideal for such searches. In particular, the signal processor allows search-mode data streams to be coherently de-dispersed at the known DM of the pulsars within the cluster. On average, the pulsars are brightest in the lowest-frequency channels, but the flux densities also vary significantly in those bands. At Parkes, the low-frequency bands are also significantly affected by RFI. Using our observations we have identified clean bands and determined the S/N of the resulting profile in those bands. The S/N is lowest in the high-frequency bands because the pulsars become weaker with increasing frequency. As the bandwidth to search increases, the time taken to complete a search also increases and therefore as a compromise between computational feasibility, sensitivity, and the ability to detect sources exhibiting an LPS spectrum, we suggest that 799–825 MHz and 970–1260 MHz are the optimal bands for independent pulsar searching with the UWL receiver at Parkes.

3.2. DM Measurements

We provide our measurements of the DM for 47 Tuc C, D, and J in Table 2 along with previous determinations from Freire et al. (2017). Our DM determinations correspond to the central MJDs 58672, 58672, and 58673 for 47 Tuc C, D, and J, respectively. Our DM measurements represent an improvement in precision over the previous measurements by about one order of magnitude. For 47 Tuc C and J, the new values are not significantly different from those obtained by Freire et al. (2017), but for 47 Tuc D the new DM deviates by more than 3σ from the previous measurement. Especially for 47 Tuc D, the pulse profile evolves significantly with frequency (discussed in Section 3.3), and we investigated if this DM deviation could result from profile evolution over our wide band. Both the use of simulated synthetic profiles and separately deriving the DM from the lower two-thirds of the band and the upper two-thirds of the band showed that the effect of profile evolution on the derived DM was negligible, at least a factor of four smaller than the quoted DM uncertainties. The observed DM variations therefore appear real and are likely to have been caused by the moving line of sight traversing electron-density irregularities in either the interstellar medium or the intracluster medium. With continued wide-band observations, providing very precise DM estimates, spanning longer time spans we will be able to monitor such DM variations in detail.

3.3. Polarization Pulse Profiles and RMs

In Figure 3, we present the mean polarization profiles of 47 Tuc C, D, and J in four different frequency bands (centered at 1792, 1152, and 832 MHz for the top three panels). We also show the average profile for a much wider band centered at 1472 MHz in the lowest panel. We note that the S/N of the profiles in the UWL sub-bands above 2240 MHz was too low to be included. The mean pulse profiles have significant linear (red line) and circular polarization (blue line). The RMs determined for each pulsar are listed in Table 2.

For 47 Tuc C, the observed pulse profiles show two components, and the amplitudes of the two components become more equal as the observing frequency increases. The trailing component has stronger linear and circular polarization than the leading component. For 47 Tuc D, the observed pulse profiles indicate three components, the leading
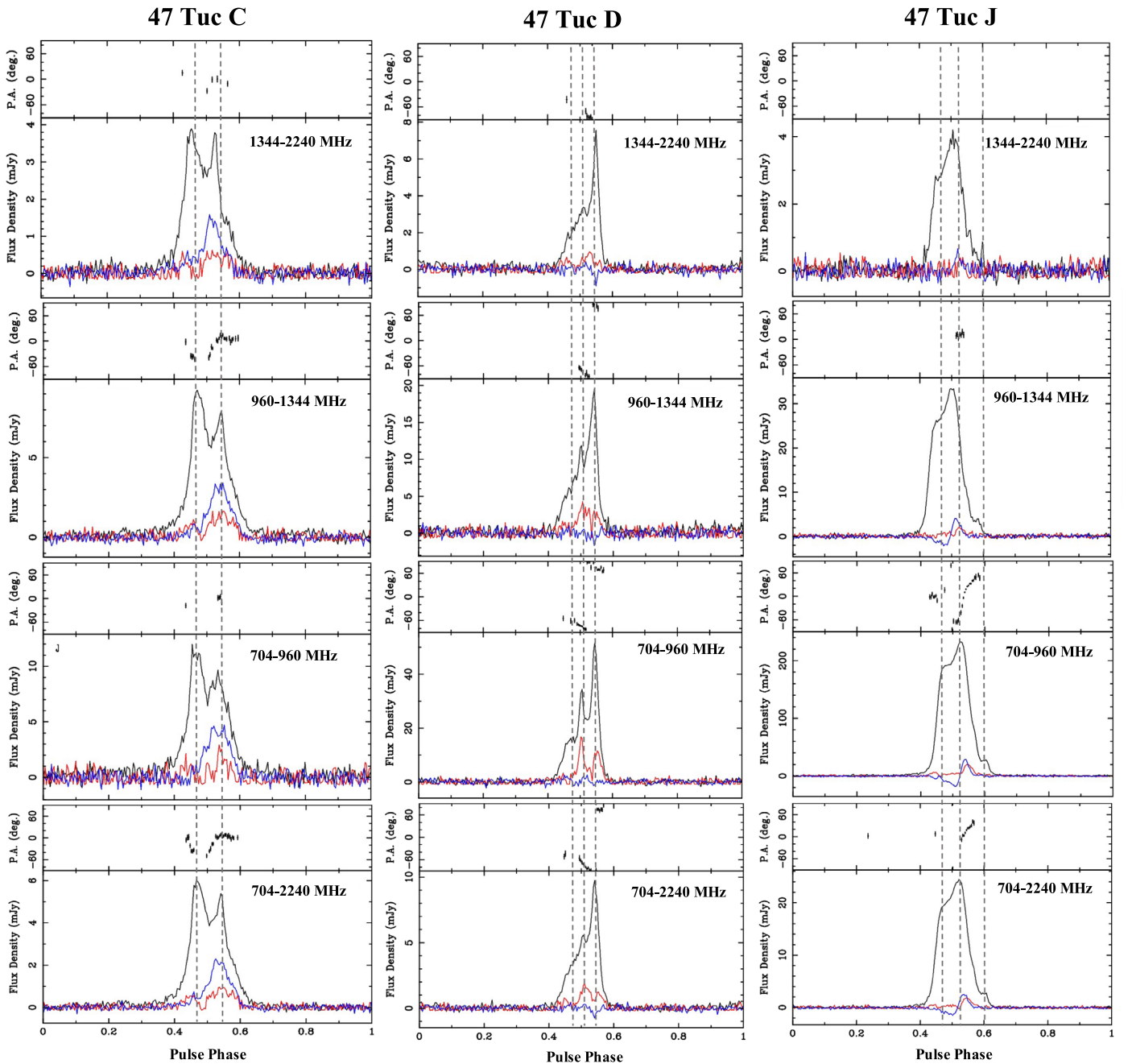
Figure 3. Average polarization profiles for 47 Tuc C, D, and J in three different frequency bands between 704 and 2240 MHz and the sum over this band. The black line is the mean flux profile, the red line is the linear polarization profile, and the blue line is the circular polarization profile. Black dots in the top panel give the linear position angle (PA) referred to the overall band center of the averaged profiles, 1472 MHz.

and central components becoming relatively weaker compared to the trailing component as the observing frequency increases. Linear polarization is clearly seen in the central and trailing components. For 47 Tuc J, the pulse profiles show three components. Linear and circular polarization is only seen in the central component.

Linear polarization and orthogonal-mode position angle (PA) jumps are commonly seen in pulsars (see, e.g., Ord et al. 2004; Dai et al. 2015). In our sample we only see evidence for an orthogonal-mode PA jump between the first and second components of 47 Tuc J (see the 704–960 MHz band in Figure 3). The PAs of 47 Tuc C (see the 930–1344 MHz band) and J (see the 704–960 MHz) vary significantly with pulse

phase and they do not allow us to fit a "rotating vector model" (RVM; Radhakrishnan & Cooke 1969). For 47 Tuc D (see the 704–960 MHz), we can fit the RVM; however, we find that the magnetic inclination angle is unconstrained and therefore we cannot fully determine the emission geometry.

Over the wide observed band, we expect to see pulse shape evolution relating to intrinsic profile changes, emission arising from different positions in the magnetosphere, and interstellar-medium and/or intracluster-medium effects. With coherently de-dispersed observations, we can obtain pulse profiles that are not affected by inter-channel DM smearing. We measured the width of the profiles for 47 Tuc C, D, and J at 50% and 10% of the peak flux density in the three observing bands centered at

832, 1152, and 1792 MHz (these results are listed in Table 2). As the observing frequency increases, the pulse widths decrease. Such reduction in profile width is well known in the general pulsar population and is usually attributed to radius-to-frequency mapping (Cordes 1978).

4. Summary and Conclusions

We have carried out the first wide bandwidth observations of pulsars C, D, and J in 47 Tuc. Flux density measurements and spectral properties (Section 3.1), updated dispersion measurements (Section 3.2), and polarization pulse profiles along with Faraday rotation measures (Section 3.3) have been presented in this Letter. We find small but significant changes in DM compared to previously published values, especially for 47 Tuc D, which probably result from the motion of the line of sight across electron-density irregularities. We will continue to observe the pulsars with the UWL receiver in order to monitor their DM and RM variations as well as building up higher-S/N polarization profiles. The observations described here were independent observations for each pulsar, but clearly a significant increase in observational efficiency would occur if we could study all the pulsars simultaneously. We can currently carry out such observations using search-mode observations, but the data volumes are prohibitive. We are therefore planning a new observing mode in which multiple pulsars (with similar DMs) can be folded online simultaneously.

ORCID iDs

Lei Zhang ● https://orcid.org/0000-0001-8539-4237
Richard N. Manchester ● https://orcid.org/0000-0001-9445-5732
Di Li ● https://orcid.org/0000-0003-3010-7661
Shi Dai ● https://orcid.org/0000-0002-9618-2499
Jingbo Wang ● https://orcid.org/0000-0001-9782-1603
Songbo Zhang ● https://orcid.org/0000-0003-2366-219X

References

Camilo, F., Lorimer, D. R., Freire, P., et al. 2000, ApJ, 535, 975
Cordes, J. M. 1978, ApJ, 222, 1006
Dai, S., Hobbs, G., Manchester, R. N., et al. 2015, MNRAS, 449, 3223
Freire, P. C., Camilo, F., Lorimer, D. R., et al. 2001, MNRAS, 326, 901
Freire, P. C. C., Ridolfi, A., Kramer, M., et al. 2017, MNRAS, 471, 857
Hobbs, G., Manchester, R. N., Dunning, A., et al. 2019, PASA, submitted
Hobbs, G., Miller, D., Manchester, R. N., et al. 2011, PASA, 28, 202
Hobbs, G. B., Edwards, R. T., & Manchester, R. N. 2006, MNRAS, 369, 655
Jankowski, F., van Straten, W., Keane, E. F., et al. 2018, MNRAS, 473, 4436
Knight, H. S. 2007, PhD thesis, Swinburne Univ. Technology
Lorimer, D. R., Camilo, F., Freire, P., et al. 2003, in ASP Conf. Ser. 302, Radio Pulsars, ed. M. Bailes, D. J. Nice, S. E. Thorsett et al. (San Francisco, CA: ASP), 363
Manchester, R. N., Lyne, A. G., D'Amico, N., et al. 1990, Natur, 345, 598
Manchester, R. N., Lyne, A. G., Robinson, C., et al. 1991, Natur, 352, 219
McConnell, D., & Ables, J. G. 2000, MNRAS, 311, 841
Ord, S. M., van Straten, W., Hotan, A. W., et al. 2004, MNRAS, 352, 804
Pan, Z., Hobbs, G., Li, D., et al. 2016, MNRAS, 459, L26
Radhakrishnan, V., & Cooke, D. J. 1969, ApL, 3, 225
Rickett, B. J. 1977, ARA&A, 15, 479
Ridolfi, A., Freire, P. C. C., Torne, P., et al. 2016, MNRAS, 462, 2918
Robinson, C., Lyne, A. G., Manchester, R. N., et al. 1995, MNRAS, 274, 547
Sobey, C., Bilous, A. V., Grießmeier, J.-M., et al. 2019, MNRAS, 484, 3646
Staveley-Smith, L., Wilson, W. E., Bird, T. S., et al. 1996, PASA, 13, 243
van Straten, W. 2004, ApJS, 152, 129
Xie, Y.-W., Wang, J.-B., Hobbs, G., et al. 2019, RAA, 19, 103
Zhang, L., Hobbs, G., Manchester, R. D., et al. 2019, Data files from the Parkes UWLreceiver system for three pulsars (C, D and J) in 47 Tuccanae, CSIRO Data Collection, doi:10.25919/5d8d7c2ee516a